Journal of Statistical Physics, Vol. 56, Nos. 5/6, 1989

Oscillatory Convection and Chaos in a Lorenz-Type Model of a Rotating Fluid

N. D. Stein[1]

Received August 25, 1988; final April 25, 1989

A four-mode model of convection in a rotating fluid layer is studied. The model is an extension of the Lorenz model of Rayleigh–Bénard convection, the extra mode accounting for the regeneration of vorticity by rotation. Perturbation theory is applied to show that the Hopf bifurcations from conductive and steady convective solutions can be either supercritical or subcritical. Perturbation theory is also used at large Rayleigh numbers r to predict novel behavior. Supercritical oscillatory convection of finite amplitude is found by numerical integration of the governing equations. The general picture is of a series of oscillatory solutions stable over large r intervals, interspersed by short bursts of chaos.

KEY WORDS: Convection; Lorenz model; rotating Rayleigh–Bénard problem; bifurcations; chaos.

1. INTRODUCTION

A productive technique for studying instabilities and chaos in fluid dynamical and other nonlinear systems is based on expansion of the variables involved as Fourier series in the spatial coordinates. Substitution in the governing partial differential equations yields a set of ordinary differential equations relating the amplitudes of the Fourier modes. By retaining only a few low-order modes, a truncated system of equations is produced which can easily be integrated on a computer. Analytic perturbation theory techniques provide supplementary information regarding small-amplitude behavior. One reason for the popularity of finite-mode truncations is that only recently has it become possible to solve the full partial differential

[1] Department of Theoretical Physics, University of Manchester, Manchester, M13 9PL United Kingdom.

0022-4715/89/0900-0841$06.00/0

equations with sufficient accuracy to detect bifurcations.[1] Moreover, it is generally impossible to follow unstable branches of the solution. In contrast, the steady branch of a finite-mode truncation can be calculated algebraically regardless of stability. Additionally, orbit-following techniques allow the bifurcation values of parameters to be pinpointed exactly, whereas in the full problem they may be masked by the effects of chaotic transients.

The prototype truncation is the so-called Lorenz model,[2]

$$\begin{aligned} \dot{x} &= \sigma(y - x) \\ \dot{y} &= -y + rx - xz \\ \dot{z} &= -bz + xy \end{aligned} \tag{1.1}$$

This models two-dimensional convection in a horizontal layer of homogeneous fluid, heated from below. Here x and y are the coefficients of the velocity and temperature modes obtained from linear theory, while z is an additional temperature mode which begins to describe the formation of thermal boundary layers. The parameters σ, r, and b are the Prandtl number, (rescaled) Rayleigh number, and a rescaled wavelength of the disturbance, respectively. For such a system it can be shown that the vertical vorticity decays exponentially to zero and can therefore be ignored.

This paper describes a related model which includes the effects of rotation about a vertical axis. Here, the vertical vorticity does not decay and is represented by an extra mode. The resulting four-mode model is the $\sigma \to \infty$ limit of the five-mode model of rotation previously considered by Veronis.[3]

Previous work includes the generalization of the Lorenz equations to a torus, carried out by Franceschini *et al.*[4,5] and Curry's[6] 14-mode extension of the basic Lorenz system. Knobloch *et al.*[7,8] have performed detailed studies of double diffusive convection and convection in an electrically conducting fluid influenced by a magnetic field. More recently, normal form theory has been used to show that behavior near multiple bifurcations may be well described by truncations involving only a small number of modes.[9,10]

Much discussion has revolved around the question of whether the limited set of modes selected adequately represents the full problem. The results of applying perturbation theory to the full problem can be replicated by first of all including the modes present in linear theory, and then adding new modes generated by substituting these linear modes into the nonlinear terms of the governing equations. If need be, additional modes may be determined by an iterative procedure, the new modes at

each step being produced by nonlinear interactions between all the modes present at the previous iteration. Knobloch *et al.*[8] observe that the truncation is only rigorously valid for small amplitudes, i.e., for values of the Rayleigh number close to the onset of convection. Second, the modes included represent two-dimensional motion, so the model will be incapable of detecting the three-dimensional instabilities which occur at large Rayleigh number in a real fluid. Third, the Lorenz system and its derivatives invariably use free boundary conditions on the upper and lower boundaries, rather than more realistic "no-slip" boundary conditions. Clever and Busse[11] show that one effect of realistic boundary conditions is to depress the maximum value of σ at which convection is first manifested as oscillations. For these reasons our model will not give accurate quantitative predictions for experimental results. Nevertheless, as the relevant physical effects have been included, we can expect the model to remain qualitatively correct beyond convective onset.

Proceeding in this spirit, Section 2 derives the equations for the four-mode model. Section 3 discusses the stability of the steady branch and the initial oscillatory branch of convection by means of perturbation theory. One advantage of the model is that the large-r behavior, though complicated, is analytically tractable using elliptic functions. This analysis is presented in Section 4. The next section deals with the numerical results in the strongly nonlinear regime, and the conclusions follow in Section 6.

2. DERIVATION OF THE MODEL

Consider a layer of fluid confined between two horizontal planes $z=0$, d maintained at temperatures $T_0+\Delta T$, T_0 respectively, and which is rotating about the vertical axis with constant angular velocity $\boldsymbol{\Omega}$. In a frame rotating with angular velocity $\boldsymbol{\Omega}$ the equations of motion in the Boussinesq approximation are[12]

$$\frac{\partial \mathbf{u}}{\partial t}+(\mathbf{u}\cdot\nabla)\,\mathbf{u}+2\boldsymbol{\Omega}\times\mathbf{u}=\alpha g T'\hat{\mathbf{z}}-\frac{1}{\rho_0}\nabla p'+\nu\nabla^2\mathbf{u} \tag{2.1}$$

$$\frac{\partial T'}{\partial t}+\mathbf{u}\cdot\nabla T'-w\frac{\Delta T}{d}=\kappa\nabla^2 T' \tag{2.2}$$

$$\nabla\cdot\mathbf{u}=0 \tag{2.3}$$

Here $\mathbf{u}=(u, v, w)$ is the fluid velocity, ν is the kinematic viscosity, κ is the thermal diffusivity, and T' and p' represent deviations in temperature and pressure, respectively, from their static distributions. The density of the

fluid is given by $\rho = \rho_0[1 - \alpha(T - T_0)]$, α being the thermal expansion coefficient.

Scaling lengths with the layer spacing d, times with the thermal diffusion time d^2/κ, velocities with κ/d, temperatures with ΔT, and pressures with $\rho_0 \nu\kappa/d^2$ produces dimensionless equations:

$$\frac{1}{\sigma}\left(\frac{\partial \mathbf{u}}{\partial t} + \mathbf{u}\cdot\nabla\mathbf{u}\right) + D\hat{\mathbf{z}}\times\mathbf{u} = RT\hat{\mathbf{z}} - \nabla p + \nabla^2\mathbf{u} \tag{2.4}$$

$$\frac{\partial T}{\partial t} + \mathbf{u}\cdot\nabla T - w = \nabla^2 T \tag{2.5}$$

where

$$R = \frac{g\alpha\,\Delta T\,d^3}{\nu\kappa}, \qquad \sigma = \frac{\nu}{\kappa}, \qquad D = \frac{2\Omega d^2}{\nu}$$

are the Rayleigh number, Prandtl number, and the square root of the Taylor number, respectively. We assume that there is no y dependence, so that the continuity equation (2.3) becomes

$$\partial_x u + \partial_z w = 0 \tag{2.6}$$

Therefore u and w can be expressed in terms of a stream function ψ as $u = \partial_z\psi$, $w = -\partial_x\psi$.

As the vorticity $\boldsymbol{\omega} = (-\partial_z v, \nabla^2\psi, \partial_x v)$, we can equally well use v as use ω_z, and the y component of (2.4) is the equivalent of the vorticity equation. Eliminating the pressure term by cross differentiating the x and z components of (2.4) yields the system of equations

$$\frac{1}{\sigma}\left[\partial_t\nabla^2\psi - J(\psi, \nabla^2\psi)\right] - D\,\partial_z v = \nabla^4\psi - R\,\partial_x T \tag{2.7}$$

$$\frac{1}{\sigma}\left[\partial_t v - J(\psi, v)\right] + D\,\partial_z\psi = \nabla^2 v \tag{2.8}$$

$$\partial_t T - J(\psi, T) + \partial_x\psi = \nabla^2 T \tag{2.9}$$

The symbol J denotes the Jacobian $J(A, B) = \partial_x A\,\partial_z B - \partial_z A\,\partial_x B$. The boundary conditions for fixed-temperature, stress-free boundaries are

$$\psi = \partial_{zz}\psi = \partial_z v = T = 0 \qquad \text{at} \quad z = 0, 1 \tag{2.10}$$

Finally, we introduce the truncated representation

$$\psi = \frac{2^{1/2}p^2}{\pi k} X(\tau) \sin \pi z \sin kx \tag{2.11}$$

$$T = -\frac{p^6}{\pi R k^2} [2^{1/2} Y(\tau) \sin \pi z \cos kx + Z(\tau) \sin 2\pi z] \tag{2.12}$$

$$v = \frac{2^{1/2}p^3}{\pi k} W(\tau) \cos \pi z \sin kx \tag{2.13}$$

where the rescaled time $\tau = p^2 t$ and $p^2 = k^2 + \pi^2$. The spatial dependence of the X, Y, and W modes comes from the eigenfunctions for the linear problem solved by Chandrasekhar,[12] while the Z mode models the formation of thermal boundary layers at the horizontal boundaries. The prefactors are chosen to simplify the final equations. Substituting this truncation into (2.7)–(2.9) and ignoring higher order Fourier components generated by nonlinear interactions gives[13]

$$\dot{X} = \sigma(Y - X + dW) \tag{2.14a}$$

$$\dot{Y} = rX - Y - XZ \tag{2.14b}$$

$$\dot{Z} = -bZ + XY \tag{2.14c}$$

$$\dot{W} = \sigma(-dX - W) \tag{2.14d}$$

in terms of a normalized Rayleigh number, wavelength, and Taylor number:

$$r = Rk^2/p^6, \qquad b = 4\pi^2/p^2, \qquad d^2 = \pi^2 D^2/p^6 \tag{2.15}$$

Note that $0 < b < 4$.

The system (2.14) possesses a spatial symmetry, for it is invariant under the transformation $(X, Y, Z, W) \to (-X, -Y, Z, -W)$, while the divergence of the system in phase space

$$\frac{\partial \dot{X}}{\partial X} + \frac{\partial \dot{Y}}{\partial Y} + \frac{\partial \dot{Z}}{\partial Z} + \frac{\partial \dot{W}}{\partial W} = -(2\sigma + b + 1) \tag{2.16}$$

is negative, so that solutions will be attracted to a set of zero measure in phase space, for example, a stationary point, limit cycle, or strange attractor.

For convenience, we make a further change in notation; (X, Y, Z, W) and τ will be written (x, y, z, w) and t in subsequent sections.

3. CONDUCTIVE AND CONVECTIVE SOLUTIONS: ANALYTIC RESULTS

3.1. Stability of the Conductive Solution

The trivial solution $x = y = z = w = 0$ of (2.14) describes the situation where heat transfer is solely by conduction, and there is no fluid motion. Its stability to infinitesimal perturbations with time dependence $\exp(\lambda t)$ may be examined by linearizing (2.14) about (0, 0, 0, 0). The z equation decouples, with solution $\lambda = -b$, which never causes instability. The other three equations give the dispersion relation

$$\lambda^3 + (2\sigma + 1)\lambda^2 + (\sigma^2 + 2\sigma - \sigma r + \sigma^2 d^2)\lambda + \sigma^2(1 + d^2 - r) = 0 \quad (3.1)$$

One real eigenvalue passes through zero when

$$r = r^{(e)} = 1 + d^2 \quad (3.2)$$

and the conducting solution loses stability to a direct mode.

A pair of complex conjugate eigenvalues crosses the imaginary axis ($\lambda = \pm i\omega_0$) when

$$r = r^{(0)} = 2(\sigma + 1) + \frac{2\sigma^2 d^2}{\sigma + 1} \quad (3.3)$$

provided that

$$\omega_0^2 = \sigma^2 \left(-1 + d^2 \frac{1 - \sigma}{1 + \sigma} \right) \quad (3.4)$$

is positive, which in turn requires

$$\sigma < \sigma_0 = \frac{d^2 - 1}{d^2 + 1} < 1 \quad (3.5)$$

In this case the conducting solution loses stability to an oscillatory mode. Since

$$r^{(e)} - r^{(0)} = \frac{2\sigma + 1}{\sigma^2} \omega_0^2 \quad (3.6)$$

two alternatives may be distinguished.

(i) $\omega_0^2 < 0$. The conduction solution is involved in exactly one bifurcation at $r = r^{(e)}$. In fact (see Section 3.2 below), it loses stability to a steady convective solution.

(ii) $\omega_0^2 > 0$. The conduction solution bifurcates at $r = r^{(0)}$ to an oscillatory convective solution. A second bifurcation occurs at $r = r^{(e)}$. However, the conduction solution remains unstable, as can be seen by tracing the behavior of the eigenvalues λ in the range $r^{(0)} < r < r^{(e)}$. At $r^{(0)}$ two complex conjugate eigenvalues acquire positive real parts. As r increases, the magnitude of their imaginary parts decreases to zero, and they become real and equal. One then decreases in order to pass through zero at $r = r^{(e)}$. The other increases and so ensures the continuing instability of the conduction solution.

3.2. The Steady Branch

Equations (2.14) have a time-independent, finite-amplitude solution

$$x = s, \qquad y = (1 + d^2)\, s, \qquad z = \frac{(1 + d^2)}{b} s^2, \qquad w = -ds \tag{3.7}$$

where

$$s^2 = b\left(\frac{r}{1 + d^2} - 1\right) \tag{3.8}$$

The solution exists provided $r > 1 + d^2$. At this point the amplitude of the solution shrinks to zero, identifying it as being involved in the pitchfork bifurcation at $r = r^{(e)}$. Two solution branches exist, given by s positive and s negative. As one branch is the image of the other under the symmetry transformation, we need only consider the case $s > 0$.

Changes to the stability of the steady convective solution above $r = r^{(e)}$ are located using linear perturbation theory, which considers infinitesimal perturbations about (3.7) with time dependence $\exp(\lambda t)$. The resulting dispersion relation is quartic,

$$\lambda^4 + a_3\lambda^3 + a_2\lambda^2 + a_1\lambda + a_0 = 0 \tag{3.9}$$

where

$$\begin{aligned} a_3 &= 2\sigma + b + 1 \\ a_2 &= A(\sigma^2 - \sigma) + 2\sigma(b + 1) + (b + s^2) \\ a_1 &= (\sigma^2 - \sigma)\, bA + \sigma s^2 A + 2\sigma(b + s^2) \\ a_0 &= 2\sigma^2 s^2 A \end{aligned} \tag{3.10}$$

and

$$A = 1 + d^2 \tag{3.11}$$

The solution $\lambda = 0$ is forbidden, because a_0 is always positive. Hence the possibility of a pitchfork bifurcation where a real eigenvalue changes sign is excluded. The other possibility is a Hopf bifurcation, obtained when $\lambda = \pm i\omega$. The real and imaginary parts of (3.9) then form two equations in s^2 and ω. The neatest way of proceeding is to use (3.8) to replace s^2 by r, then eliminate r via the relation

$$r = \frac{1}{A+2}\left[\frac{2\sigma+b+1}{\sigma b} A\omega^2 - (\sigma-2)A^2\right] \tag{3.12}$$

The end product is a quadratic equation for ω^2,

$$\alpha\omega^4 + \beta\omega^2 + \gamma = 0 \tag{3.13}$$

where

$$\begin{aligned} \alpha &= \sigma A - b - 1 \\ \beta &= -A(A+2)\sigma^2(\sigma-1) + 4\sigma^2\alpha + \sigma bA(\sigma-2) \\ \gamma &= -2\sigma^3 bA[(\sigma-1)A+2] \end{aligned} \tag{3.14}$$

Simple considerations regarding the number of real, positive roots of ω^2 in (3.13) determine how many Hopf bifurcations occur. The results are summarized in Table I.

Inverting (3.8) to give r as a function of the amplitude s shows that the bifurcation is supercritical and the curve $r(s)$ contains no turning points. A general result[7] states that if Hopf bifurcations are excluded, the steady branch can only change its stability at $r = r^{(e)}$ or a turning point. This confirms our previous observation that an eigenvalue cannot pass through zero above $r = r^{(e)}$. We are now in a position to give a complete description of the stability of the steady branch. Various different cases can be distinguished by tracing the evolution of the eigenvalues of (3.9). The techniques are standard,[8] so we omit the details and illustrate the results in Fig. 1. Note that Eq. (3.10) constrains the sum of the eigenvalues to be

Table I. Number of Hopf Bifurcations Occurring on the Steady Branch

	$\sigma > 1$	$\sigma_0 < \sigma < 1$	$\sigma < \sigma_0$
$\sigma > (b+1)/(d^2+1)$	1	1	0 or 2
$\sigma < (b+1)/(d^2+1)$	0	0 or 2	1

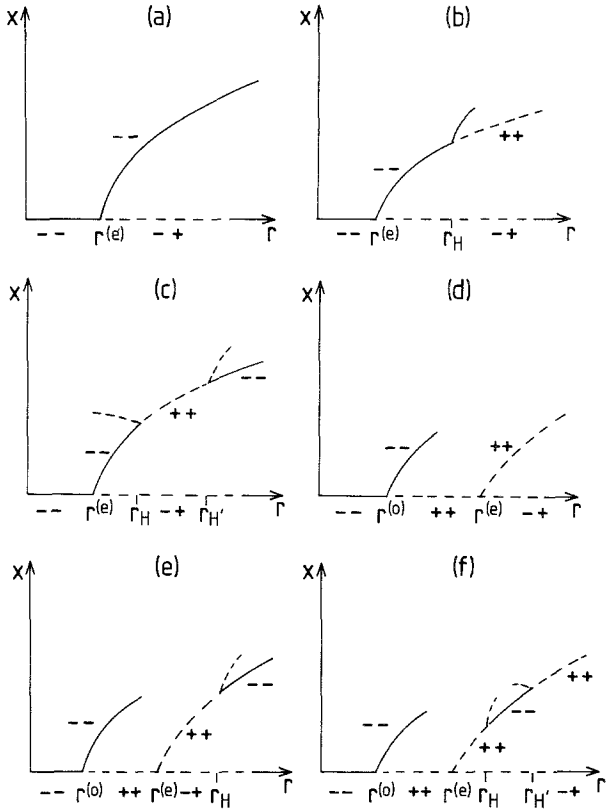

Fig. 1. Evolution of the steady branch in the r-amplitude plane. (a–c) No oscillatory branch ($\omega_0^2 < 0$) and 0, 1, 2 Hopf bifurcations on the steady branch. (d–f) The steady branch is rendered initially unstable by the presence of the oscillatory branch. Broken lines represent unstable solutions. The plus and minus signs denote the signs of the real parts of the two significant eigenvalues of the linearized flow. The remaining two eigenvalues always have negative real parts. In panels (b), (e), and (f) the bifurcations at r_H, $r_{H'}$ can be in opposite directions to those shown.

negative. This consideration leads to the restabilization of the steady branch at the second Hopf bifurcation in Fig. 1c and at the first Hopf bifurcation in Figs. 1e and 1f.

3.3. Stability of Oscillatory Solutions Bifurcating from Conduction and Steady Convection

Although large-amplitude oscillations can only be studied by integrating equations (2.14) numerically, the behavior of the oscillatory branch in

the neighborhood of the onset of convection at $r = r^{(0)}$ is accessible via modified perturbation theory. Details of the calculation appear in Appendix A. It is found that the bifurcation to oscillations can be either supercritical or subcritical, depending on the values of σ, b, and d. The Hopf bifurcation theorem tells us that a supercritical bifurcation leads to stable oscillatory motion above $r = r^{(0)}$. This is the case for the parameter values examined numerically in Section 5. However, subcritical bifurcations may also occur, particularly for large values of the Taylor number d^2. A branch of unstable oscillatory solutions then exists for $r < r^{(0)}$. If this branch subsequently gains stability by reversing direction toward large r, finite-amplitude oscillations may be observed immediately above $r = r^{(0)}$.

The Hopf bifurcation from steady convection at $r = r_H$ can be examined in a similar way. It has been shown that, in the Lorenz model, this bifurcation is subcritical for all choices of parameter values.[15] Above $r = r_H$, solutions of the Lorenz equations are chaotic, at variance with experiment and the solutions of the full partial differential equations, which show stable oscillations, indicating the presence of a supercritical bifurcation. Curry's extension[6] of the Lorenz model to 14 modes reproduced the supercritical behavior. It is of interest to determine whether the addition of rotation to the basic Lorenz model can reverse the direction of the bifurcation. We proceed by applying modified perturbation theory.

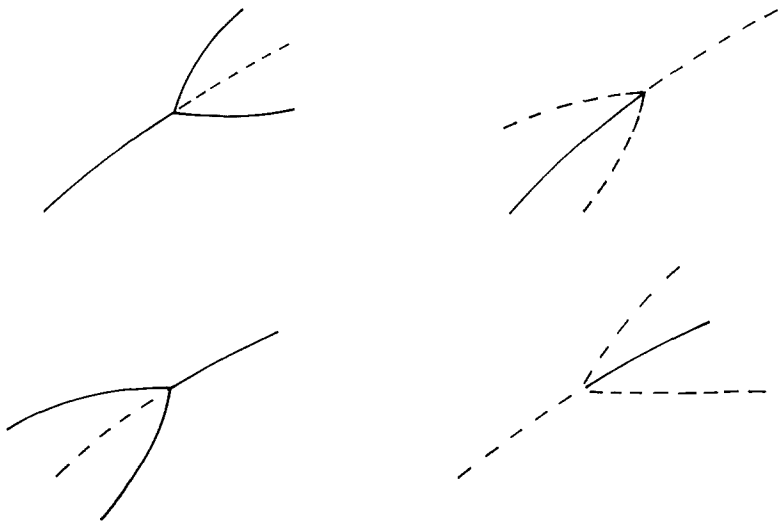

Fig. 2. The four types of Hopf bifurcation from the steady branch. Broken lines denote unstable solution branches. The oscillatory solutions have opposite stability to the coexisting part of the stationary branch.

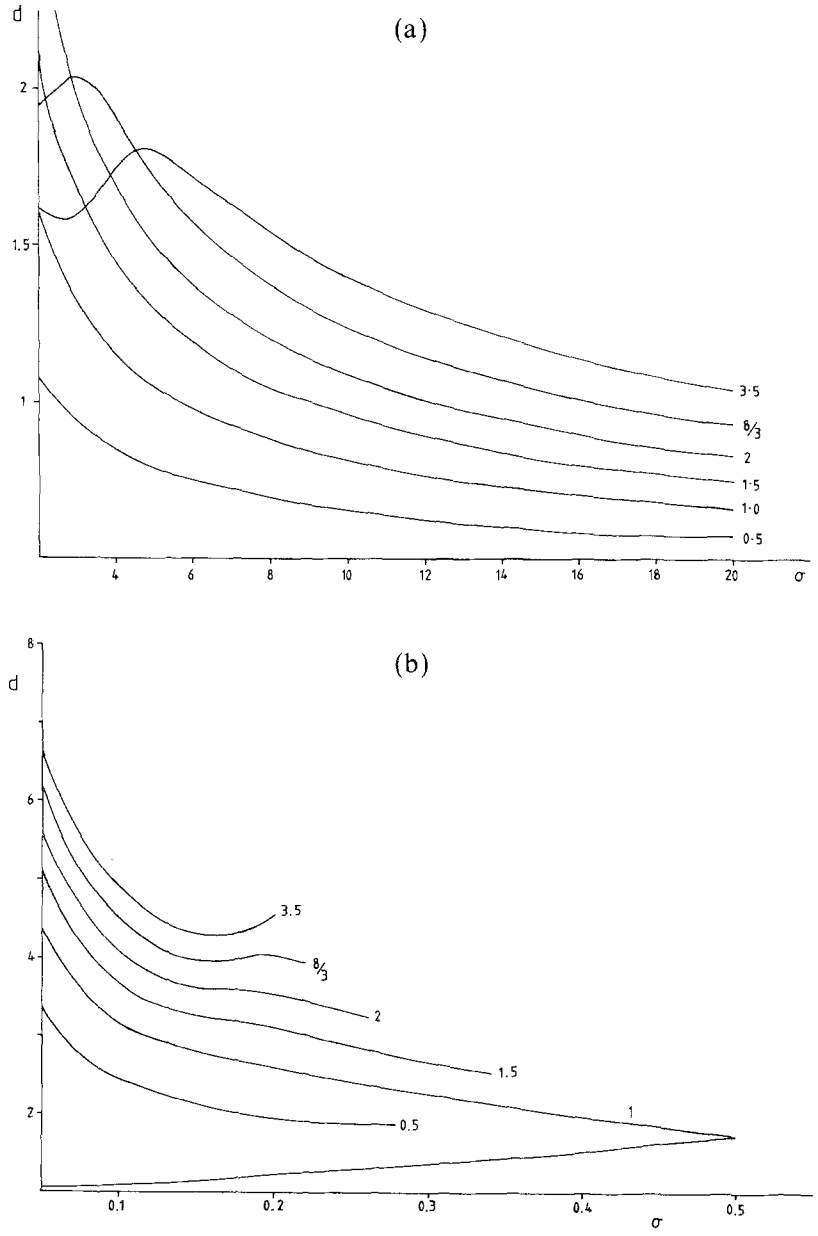

Fig. 3. Values of d at which $s_2 = 0$, marking a transition between subcritical and supercritical bifurcations. The curves are labeled with the value of b. (a) $\omega_0^2 < 0$. (b) $\omega_0^2 > 0$, and the $b = 1$ curve ends on the line $\omega_0^2 = 0$. The other curves terminate when $\sigma = (b+1)/(d^2+1)$ and the bifurcation ceases to exist.

Suppose the Hopf bifurcation occurs at the point $s = s_0$ (see Eq. 3.7). It is convenient to use s rather than r as parameter to avoid the need to take square roots. A nearby point on the steady branch is given by

$$s = s_0 + \varepsilon^2 s_2 + \cdots \tag{3.15}$$

and r is recovered from (3.8),

$$r = (1 + d^2)\left[1 + \frac{1}{b}(s_0^2 + 2\varepsilon^2 s_0 s_2) + O(\varepsilon^4)\right] \tag{3.16}$$

We assume periodic motion for perturbations about this point:

$$\frac{d}{dt}(x - s) = i\omega(x - s) \tag{3.17}$$

and similarly for the other variables.

As the calculation now proceeds just as before, only the result is quoted in Appendix A. Again the bifurcation can be in either direction (see Fig. 2). From (3.16) it is forward if $s_2 > 0$ and backward if $s_2 < 0$. Although two Hopf bifurcations can sometimes occur (Figs. 1c and 1f), the discussion below concentrates on the first bifurcation, at $r = r_H$.

If d is increased with $\sigma > 1$, s_2, although initially negative, rapidly rises to pass through zero at $d \sim 1$. Shortly afterward it reaches a maximum and then slowly decays. If $\sigma < \sigma_0$, s_2 starts off negative and becomes positive at a somewhat larger value of d, provided σ is small enough. This time the transition is from stable to unstable oscillatory solutions with increasing d. For larger values of σ, s_2 remains negative throughout. The values of d at the transition between subcriticality and supercriticality are plotted in Fig. 3. The intermediate case $1 > \sigma > \sigma_0$ is more complicated; s_2 can be either positive or negative at small d and a change of sign may or may not take place, depending on the values of σ and b. However, when two Hopf bifurcations occur, both always appear to be subcritical, as drawn in Fig. 1c. Thus, both oscillatory solution branches are initially unstable.

4. BEHAVIOR AT LARGE r

In the limit $r \to \infty$, the system (2.14) can be analyzed by treating $\varepsilon = r^{-1/2}$ as a small parameter. We will see that the large-r results so obtained yield useful constraints on the behavior at smaller values of r. The discussion in this section relies heavily on the analogous treatment of the Lorenz equations in Sparrow's book.[16]

The relative magnitudes of the variables at large r are found by considering the function

$$V = rx^2 + \sigma y^2 + \sigma(z-2r)^2 + rw^2 \tag{4.1}$$

which has time derivative

$$\frac{dV}{dt} = -2\sigma[rx^2 + y^2 + b(z-r)^2 + rw^2 - br^2] \tag{4.2}$$

Let D be the ellipsoidal region inside which $dV/dt \geqslant 0$ and let E be the region $V \leqslant c + \delta$, where c is the maximum of V in D and δ is small, positive. A phase space point $\mathbf{x} = (x, y, z, w)$ which lies outside E must also lie outside D and hence satisfies $\dot{V}(\mathbf{x}) \leqslant -\delta'$, where δ' depends on δ. A trajectory commencing at $\mathbf{x}$ will eventually enter E and subsequently remain inside E.

Since surfaces of constant V are ellipsoids centered on $(0, 0, 2r, 0)$, it is clear that the maximum of V in D lies on the boundary of D. Maximizing V subject to the constraint

$$rx^2 + y^2 + b(z-r)^2 + rw^2 = br^2 \tag{4.3}$$

results in three alternatives:

$$\begin{aligned}
&\text{(i)} \quad V_{\max} = \frac{\sigma r^2 b^2}{b-1} \qquad \text{if} \quad b \geqslant 2, \quad \sigma \geqslant 1 \\
&\text{(ii)} \quad V_{\max} = \frac{r^2 b^2}{b-\sigma} \qquad \text{if} \quad b \geqslant 2\sigma, \quad \sigma \leqslant 1 \\
&\text{(iii)} \quad V_{\max} = 4\sigma r^2 \qquad \text{otherwise}
\end{aligned} \tag{4.4}$$

In each case the maximum of V in D, and hence also the maximum of V in E, is $O(r^2)$. Comparing (4.1), we see that

$$x = O(r^{1/2}), \qquad y = O(r), \qquad z = O(r), \qquad w = O(r^{1/2}) \tag{4.5}$$

This suggests the rescaling

$$\begin{aligned}
&\varepsilon = r^{-1/2}, \qquad x = \varepsilon^{-1}\xi, \qquad y = \varepsilon^{-2}\sigma^{-1}\eta \\
&z = \varepsilon^{-2}(\sigma^{-1}Z + 1), \qquad w = \varepsilon^{-1}\mu, \qquad t = \varepsilon\tau
\end{aligned} \tag{4.6}$$

where the new variables (ξ, η, Z, μ) are $O(1)$. Substitution in (2.14) gives

$$\frac{d\xi}{d\tau} = \eta - \varepsilon\sigma\xi + \varepsilon\sigma d\mu \tag{4.7a}$$

$$\frac{d\eta}{d\tau} = -\xi Z - \varepsilon\eta \tag{4.7b}$$

$$\frac{dZ}{d\tau} = \xi\eta - \varepsilon b(Z+\sigma) \tag{4.7c}$$

$$\frac{d\mu}{d\tau} = -\varepsilon\sigma\mu - \varepsilon\sigma d\xi \tag{4.7d}$$

In the limit $\varepsilon \to 0$, Eqs. (4.7) become

$$\frac{d\xi}{d\tau} = \eta \tag{4.8a}$$

$$\frac{d\eta}{d\tau} = -\xi Z \tag{4.8b}$$

$$\frac{dZ}{d\tau} = \xi\eta \tag{4.8c}$$

$$\frac{d\mu}{d\tau} = 0 \tag{4.8d}$$

These equations have three first integrals,

$$\begin{aligned} \xi^2 - 2Z &= 2A \\ \eta^2 + Z^2 &= B^2 \\ \mu &= C \end{aligned} \tag{4.9}$$

where $B \geqslant 0$ and $A \geqslant -B$.

Equations (4.8) can now be integrated to express (ξ, η, Z, μ) in terms of τ and the three constants A, B, and C. Details of this calculation, involving the use of Jacobian elliptic functions, appear in Appendix B together with a detailed derivation of the averaged equations. Returning now to the situation when $\varepsilon \neq 0$, we expect A, B, and C to be slowly varying rather than constant. Indeed, differentiating (4.9) and using the exact equations (4.7) gives

$$\begin{aligned} A' &= \varepsilon(-\sigma\xi^2 + bZ + b\sigma + \sigma d\mu\xi) \\ BB' &= -\varepsilon(\eta^2 + bZ^2 + b\sigma Z) \\ C' &= -\varepsilon(\sigma\mu + \sigma d\xi) \end{aligned} \tag{4.10}$$

confirming that the time derivatives are all $O(\varepsilon)$. Appendix B demonstrates

explicitly that the solutions of the $\varepsilon = 0$ equations are periodic orbits. We may therefore apply the method of averaging and integrate (4.10) over one period of the $\varepsilon = 0$ equations. This procedure gives average values for A', B', and C' (in terms of A, B, and C) relating to the full ($\varepsilon \neq 0$) equations (4.7). Stationary points of the averaged equations correspond to periodic orbits in the original variables. Degenerate cases, e.g., $B = 0$, give stationary points of the original equations rather than periodic orbits.

The results of the calculations in Appendix B can be summarized as follows.

(i) Introducing a parameter $\lambda = (\sigma + 1)/(b + 2)$, we find that if $\lambda > 2/3$, there is a stable symmetric orbit at large r. Otherwise, no stable orbit persists to large r. This is exactly the same result as for the standard Lorenz model.[16]

(ii) If $\sigma > (b + 1)/(d^2 + 1)$, one pair of nonstable, asymmetric orbits exists at large r.

If $(b + 1)/(d^2 + 1) - \varepsilon' < \sigma < (b + 1)/(d^2 + 1)$ and $d^2 < (b + 2)/b$, two pairs of nonstable, asymmetric orbits exist at large r. The parameter ε' is in principle a function of b and d, and is small. Otherwise there are no nonstable orbits at large r.

(iii) The averaged equations have a stationary point at $A = b/2(1 + d^2)$, $B = 0$. Following Sparrow,[16] we identify this stationary point with the two stationary points of the original equations which signify the two branches of the steady convective solution. If $\sigma < (b + 1)/(d^2 + 1)$ trajectories with B small, positive move toward the stationary point. This ties in nicely with the work of Section 3.2, because if $\sigma < (b + 1)/(d^2 + 1)$, then for $r^{(e)} < r^{(0)}$, the steady branch undergoes zero or two Hopf bifurcations and is stable at large r. Conversely, if $r^{(0)} < r^{(e)}$, the steady branch ends up stable at large r through restabilization at a single Hopf bifurcation.

The origin of these asymmetric orbits is not as clear-cut as in the Lorenz model. The situation with $\sigma > (b + 1)/(d^2 + 1)$ corresponds to types (b), (d), and (f) of Fig. 1. In type (b) the large-r orbits may originate from the Hopf bifurcation at r_H, while in type (d) they may come from the oscillatory branch which starts at $r^{(0)}$, provided it subsequently undergoes a symmetry-breaking bifurcation. Types (a), (c), and (e) may all arise if $\sigma < (b + 1)/(d^2 + 1)$. We expect type (a) to produce no orbits at large r because the stationary branch is forever stable. If $\sigma > \sigma_0$ the possibility of two orbit pairs at large r seems to be related to the appearance of type (c) behavior, the two pairs being remnants of the bifurcations at r_H and r'_H respectively. However, two pairs can still be produced if $\sigma < \sigma_0$.

For the standard Lorenz model one pair of nonstable, nonsymmetric orbits exists if $2/3 < \lambda < 1$; otherwise there are none. The radically different result obtained here for the rotating fluid layer is essentially due to a logarithmic singularity in the term proportional to d^2 in the equation (B12) which determines stationary points of the averaged equations. This term can therefore become dominant regardless of the size of d, provided d is not zero.

5. CHAOTIC AND OSCILLATORY NONLINEAR SOLUTIONS

When nonlinear effects are large, Eqs. (2.14) must be solved by numerical integration. It is convenient to view the solutions as trajectories in four-dimensional phase space. From this viewpoint an oscillatory solution forms a closed orbit in phase space. Our study makes use of powerful orbit-following techniques devised by Curry[18] and described in detail by Sparrow.[16]

An important feature of the orbit-following program lies in its ability to follow orbits as r changes. Were the solution to be computed afresh for each r, much time would be wasted waiting for transients to decay. The technique also allows precise determination of parameter values at which bifurcations occur. Examination of Floquet multipliers permits us to distinguish among saddle-node, symmetry-breaking and period-doubling bifurcations.

The necessary integrations were performed by a fourth-order Runge-Kutta method with varying timesteps, using NAG routines D02BAF and D02BBF.

5.1. The Regime Where the Conduction Solution First Loses Stability to Oscillatory Convection

We consider in detail the case $\sigma = 0.5$, $b = 2$, $d = 3$, so that $r^{(0)} = 6$, $r^{(e)} = 10$, and Eqs. (3.9)–(3.14) reveal the steady convective branch to be unstable for all r and as such unlikely to exert any influence on the observed motion. The Hopf bifurcation at $r = 6$ is supercritical and stable oscillatory motion is observed for $r > 6$. At first the amplitude of the solution increases rapidly with increasing r, as the oscillations evolve away from the sinusoidal form predicted by perturbation theory. As r increases further, the period and amplitude of the solution, which we label orbit A, change much more slowly. As predicted in Section 3, the orbit is symmetric, and it remains stable until $r \approx 27.14$, where it loses stability in a symmetry-breaking bifurcation. The now unstable orbit continues in

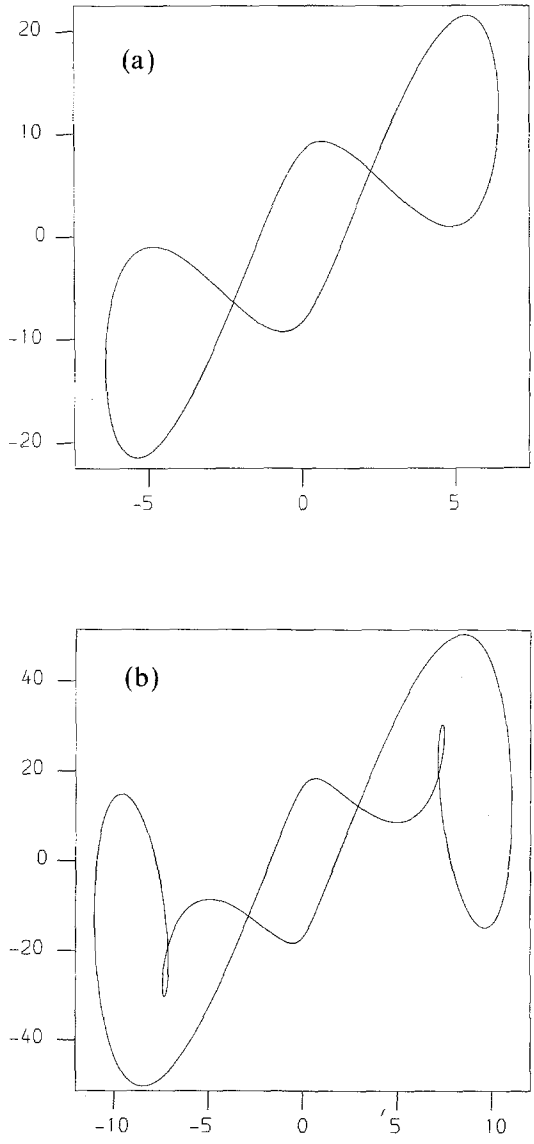

Fig. 4. Limit cycles when $\sigma = 0.5$, $b = 2$, $d = 3$, plotted in the x–y plane. (a) Orbit A, $r = 24$, period 5.06. (b) Orbit B, $r = 57$, period 5.38. (c) Orbit C, $r = 57$, period 8.36. (d) Orbit D, $r = 62$, period 8.59. (e) Orbit E, $r = 63.5$, period 11.39. (f) Orbit F, $r = 38.685$, period 9.02.

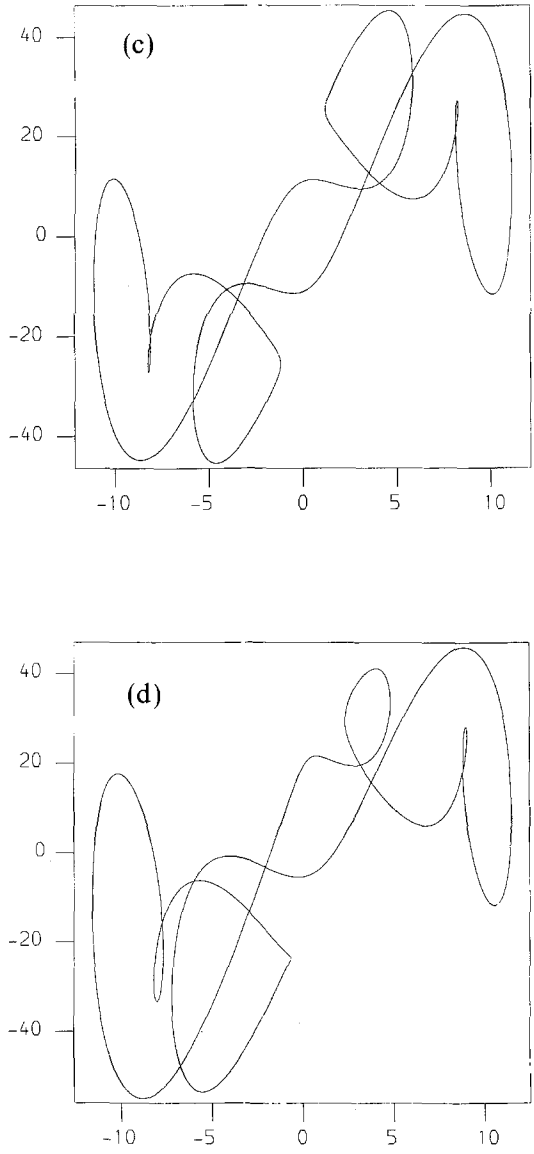

Fig. 4 (*continued*)

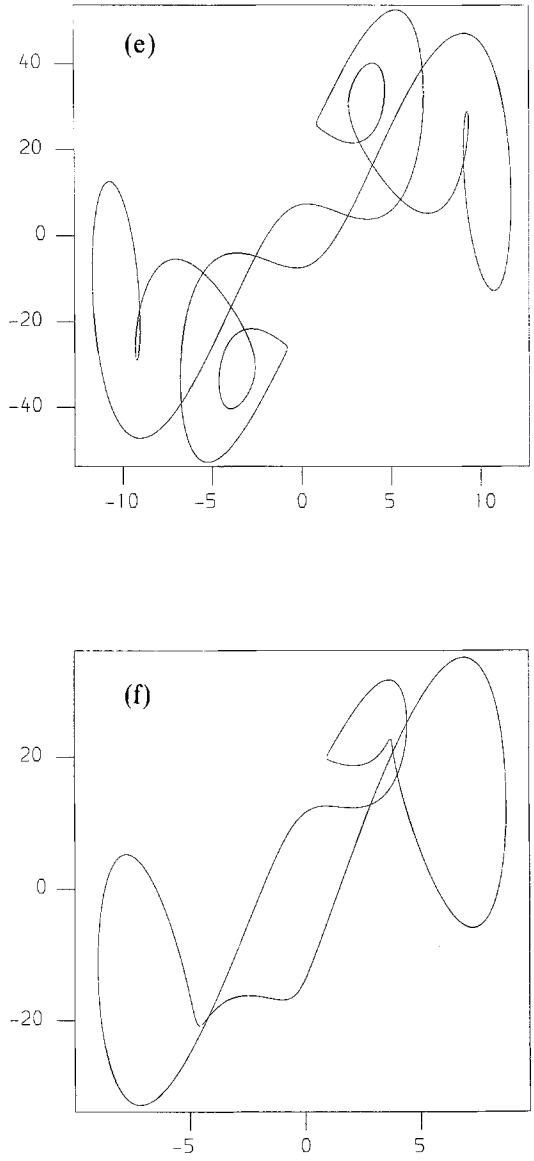

Fig. 4 (*continued*)

existence beyond $r = 38$, at which point its period is steadily increasing and the orbit-following program has difficulty converging, both factors suggesting that it is approaching homoclinicity. [Strictly speaking, orbit A becomes nonstable rather than unstable at $r \approx 27.14$, i.e., the flow linearized about the orbit has at least one positive and one negative eigenvalue. No solution of (2.14) can be unstable, because then the flow in a neighborhood of that solution would be locally expanding, which contradicts (2.16). However in this paper the terms unstable and nonstable will be used interchangeably.] Integration of (2.14) above the bifurcation value produces chaotic solutions (Fig. 6) even for r values differing from the bifurcation value by only 10^{-4}. We hypothesize that the symmetry-breaking bifurcation is in the backward direction. The pair of nonsymmetric orbits involved would then be unstable and difficult to detect. The general form of orbit A is illustrated in Fig. 4a, while Fig. 5 shows schematically the ranges of stability of all the oscillatory solutions found.

Two more symmetric orbits are created simultaneously in a saddle-node bifurcation at $r = 43.06$, one of which (labeled B) is stable. Solutions of (2.14) starting at an arbitrary point in phase space eventually converge

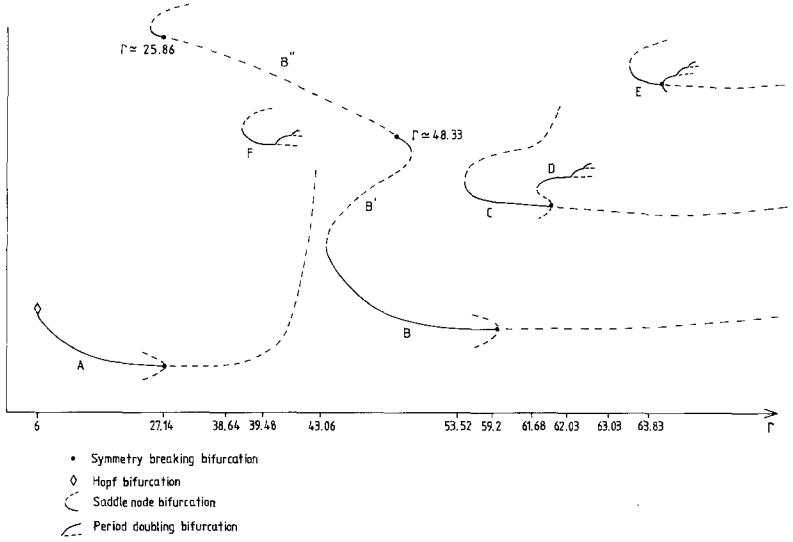

Fig. 5. The various oscillatory solutions present at $\sigma = 0.5$, $b = 2$, $d = 3$. The branches of orbit B and the other major orbits A, C, D, and E are arranged so that period increases along the vertical axis. Owing to the limitations of a two-dimensional representation, the same is not true for the details of the figure; for example, the two asymmetric orbits participating in a symmetry-breaking bifurcation are images of each other under the symmetry and so have equal period for all r.

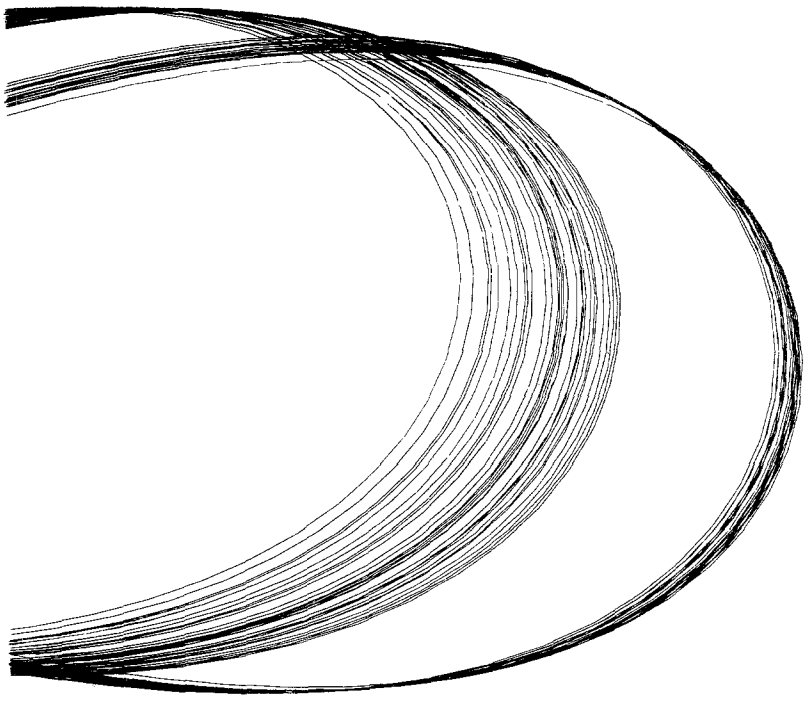

Fig. 6. Chaotic solution obtained immediately above the stable range of orbit A, at $r = 27.1327$.

onto this orbit. At the bifurcation value r_0, suppose $\mathbf{x}$ is the intersection of orbit B with a given return plane and τ is the orbital period. When $r = r_0 + \delta r$, let the corresponding quantities be $\mathbf{x} + \delta\mathbf{x}$, $\tau + \delta\tau$. Then the unstable partner orbit B' can also be located, because at $r = r_0 + \delta r$, a point lying on this orbit is $\mathbf{x} - \delta\mathbf{x}$ and the orbital period is $\tau - \delta\tau$, to first order in small quantities. These initial guesses are sufficiently good to enable the orbit-following program to converge onto B'. Orbit B remains stable until it participates in a symmetry-breaking bifurcation at $r \approx 59.2$. Meanwhile, orbit B' can be traced up to $r = 48.33$, where a further saddle-node bifurcation ensues. A new stable partner orbit can be found in the same way as above and can be followed, with decreasing r this time, to $r \approx 25.86$, where yet another saddle-node bifurcation occurs. Such behavior, particularly when sketched in the r–τ plane (Fig. 5), strongly resembles the oscillatory approach to a homoclinic orbit investigated theoretically by Glendinning and Sparrow.[19] In theory, further branches of this solution could be followed between saddle node bifurcations by alternately increasing and decreasing r. However, in practice the orbit labeled B'' in Fig. 5 is already

violently unstable throughout most of its range of existence, one of the Floquet multipliers becoming very large. Note that although B'' is (just) stable in the immediate vicinity of the two saddle node bifurcations, it quickly loses stability via symmetry-breaking bifurcations, a phenomenon previously observed in other systems.[19] Thus, it proved impossible to converge onto solution branches of higher period.

Solutions in the range $27.14 < r < 43.06$ are generally chaotic, although a myriad of narrow periodic windows is imbedded in the chaotic region. By far the shortest period of these is orbit F, an asymmetric orbit born in a saddle-node bifurcation at $r \approx 38.64$ and persisting until $r = 39.48$, where there is a transition back to chaos via a period-doubling cascade, the first few period doublings occurring at $r = 39.48$, $r = 39.49$, $r = 39.4909$. The other periodic windows occupy narrower r intervals. Some of the shorter period examples found are listed in Table II.

Proceeding now to the situation above $r = 59.2$, where orbit B has become unstable, solutions starting in the vicinity of orbit B do not eventually converge onto an antisymmetric orbit of similar period. This leads to the hypothesis that the symmetry-breaking bifurcation at $r = 59.2$ is again subcritical, with the asymmetric orbit pair produced being unstable. (Since two unstable orbits are involved, we cannot predict their positions and periods using the first-order methods which were successful at saddle-node bifurcations.) Instead, solutions immediately above the symmetry-breaking bifurcation approach another symmetric orbit of higher period, orbit C. This stable orbit can be followed with increasing r up to $r \approx 61.87$, where it surrenders its stability in a symmetry-breaking bifurcation, but it can also be followed with decreasing r until it is annihilated in a saddle-node

Table II. Some of the Periodic Windows in the r Interval between Orbit A Losing Stability and the Appearance of Orbit B, for $\sigma = 0.5$, $b = 2$, $d = 3$[a]

Stable r range	Number of loops	Symmetry
38.00–38.12	5	S
39.66–39.95	5	S
40.27–40.93	3	S
40.98–41.08	7	S
41.14–41.61	3	A
41.70–42.02	5	S
42.45–42.56	4	A

[a] The number of loops executed in the x–w plane before the orbit closes on itself provides a measure of orbital period. S, A stand for symmetric and asymmetric, respectively.

bifurcation at $r = 53.52$. Hence, over the range $53.52 < r < 59.2$, two distinct orbits B and C are simultaneously stable.

Above $r = 61.87$, solutions snap through to orbit D. Although orbit D is asymmetric, it cannot be directly involved in the symmetry-breaking bifurcation because its period is approximately 8.53 dimensionless units, appreciably different from orbit C, whose period is ~ 8. Neither is there a Floquet multiplier 1 at $r = 61.87$. That orbits C and D are, nevertheless, closely related can be seen by tracing D back to a saddle-node bifurcation at $r \approx 61.675$, by which time its period has dropped to 8.23. Its unstable partner orbit D' has shorter period and as r approaches 61.87 the period tends to 8.0 and the largest Floquet multiplier tends to 1, confirming that D' is indeed one of the asymmetric orbits produced in the symmetry-breaking bifurcation, the other being the image of D' under the symmetry transformation. The interaction between C and D is summarized in Fig. 7 and provides an explicit demonstration that the symmetry-breaking bifurcation which terminates the stable range of orbit C is backward. Contrast the situation regarding orbits A and B, where some doubt always exists owing to the possibility of a supercritical period-doubling cascade occurring in some arbitrarily small interval of r values immediately following the bifurcation. Orbit D ultimately loses stability in a period-doubling cascade, the doubled orbit appearing at $r \approx 62.03$. The next two bifurcations to quadrupled and eightfold orbits take place at $r \approx 62.092$ and $r \approx 62.105$, respectively. After the accumulation point of the period doublings, there is an

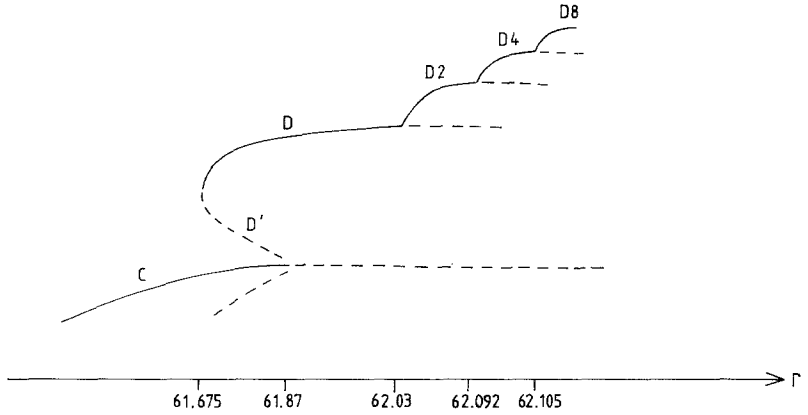

Fig. 7. Details of the interaction between orbits C and D. The only symmetric orbit present, orbit C, goes unstable in a backward symmetry-breaking bifurcation, involving orbit D'. Orbits D and D' emanate from the same saddle-node bifurcation. Orbit D ultimately loses stability in a period-doubling cascade. Hysteresis can be observed between $r = 61.675$ and $r = 61.87$.

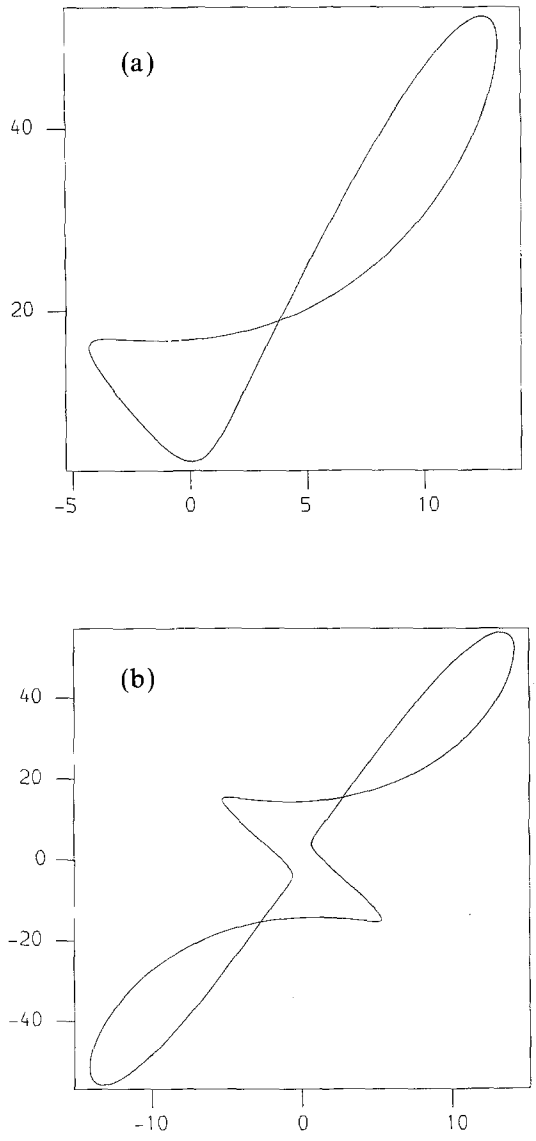

Fig. 8. Limit cycles when $\sigma = 4$, $b = 8/3$, $d = 2.5$, plotted in the x–y plane. (a) Asymmetric orbit A, $r = 63$, period 0.96, (b) symmetric orbit B, $r = 65.9$, period 2.04, (c) symmetric orbit C, $r = 80$, period 3.18.

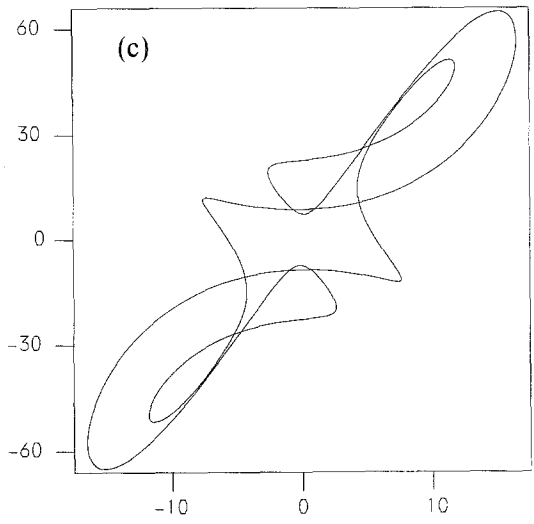

Fig. 8 (*continued*)

inverse cascade of chaotic solutions which exhibits noisy periodicity, followed by fully developed chaos. Solutions for still larger values of r remain chaotic until, at $r \approx 63.03$, yet another saddle node bifurcation takes place, generating a stable symmetric orbit E of higher period than orbits C and D (Fig. 4e), and its unstable partner, orbit E'. Orbit E also loses stability through a period-doubling cascade in the forward direction. The symmetry-breaking bifurcation, a necessary precursor to period doubling, occurs at $r \approx 63.83$, with a relatively widely spaced sequence of period doublings, the first three being at $r \approx 64.55$, $r \approx 64.67$, and $r \approx 64.70$.

Table III. Bifurcation Values of r for the First Few Period Doublings for Orbits A, B, C when $\sigma = 4$, $b = 8/3$, $d = 2.5$[a]

	A	*B*	*C*
S → A	NA	65.97	81.2
1 → 2	63.776	70.074	83.790
2 → 4	63.846	70.8410	94.2828
4 → 8	63.8584	71.0045	84.3889
8 → 16	63.86097		
16 → 32	63.86152		

[a] S → A indicates the symmetry-breaking bifurcation, which applies only to an initially symmetric orbit; 1 → 2 indicates period doubling, 2 → 4 period quadrupling, etc.

The unstable continuations of orbits B, C, and E together with the unstable orbits C' and E' were followed with increasing r until in each case the orbit-locating program had difficulty in converging, partly due to an increase in orbital period. Often this did not happen until a considerable r interval had elapsed. It seems that these orbits eventually disappear in homoclinic bifurcations.

5.2. The Regime Where the Conduction Solution Loses Stability to Stationary Convection

We concentrate on the parameter values $\sigma = 4$, $b = 8/3$, $d = 2.5$. The value of d is chosen to give a large, positive value of r_2 at the Hopf bifurcation from steady convection and so maximize the likelihood of observing supercritical stable oscillations. At the same time, d is not so large that interesting behavior only occurs at inconveniently high values of r.

The conduction solution is stable until $r = 7.25$ and trajectories in phase space tend to the stationary point at the origin. The steady convective solution is stable for r values above 7.25 but below the Hopf bifurcation value of $r \approx 61.02$. Trajectories spiral in to one of the stationary points given by Eqs. (3.7) and (3.8). Beyond the Hopf bifurcation stable oscillatory motion is indeed observable (orbit A) until, at $r = 63.78$, the asymmetric orbit A loses stability in a period-doubling bifurcation. Further, rather tightly spaced period-doubling bifurcations follow and immediately beyond $r \approx 63.86$, the solution is chaotic.

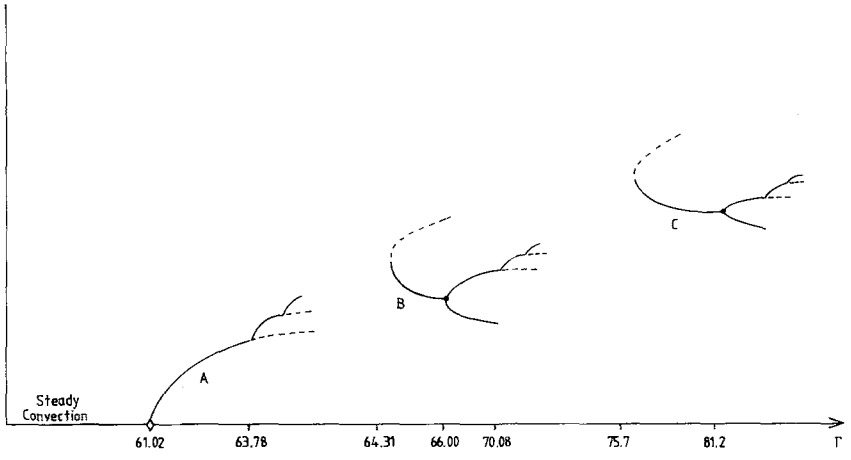

Fig. 9. Schematic bifurcation diagram for $\sigma = 4$, $b = 8/3$, $d = 2.5$.

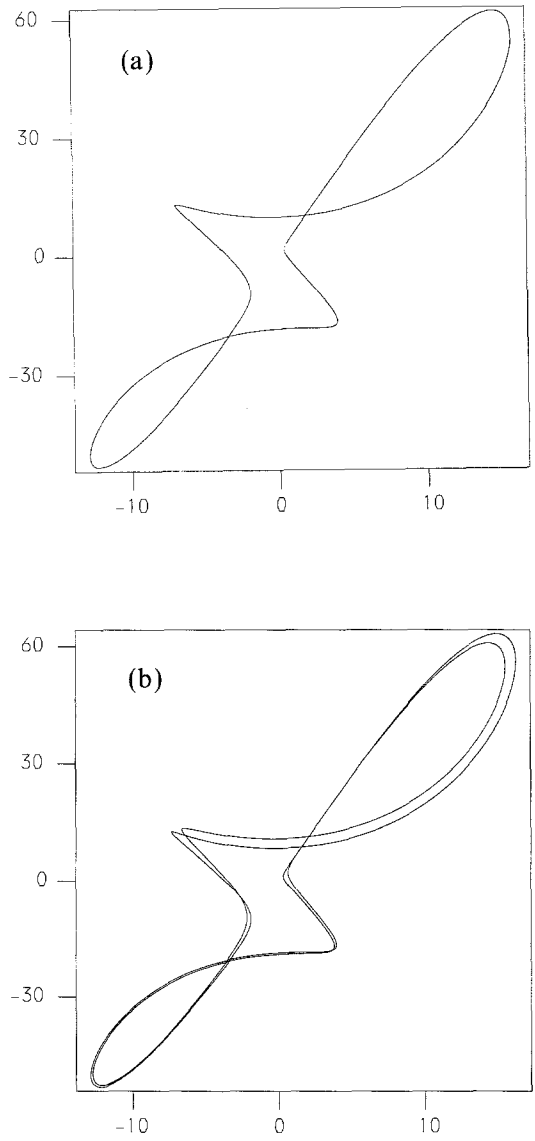

Fig. 10. The transition between stable symmetric orbit B and chaos. (a) Nonsymmetric solution at $r = 70.05$. (b) Doubled solution at $r = 70.80$. (c) $r = 71.17$, noisy periodicity. (d) Fully developed chaos at $r = 73.00$.

(c)

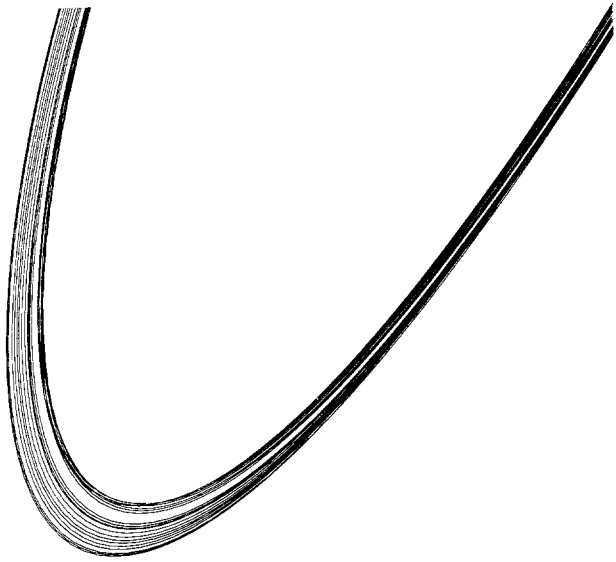

(d)

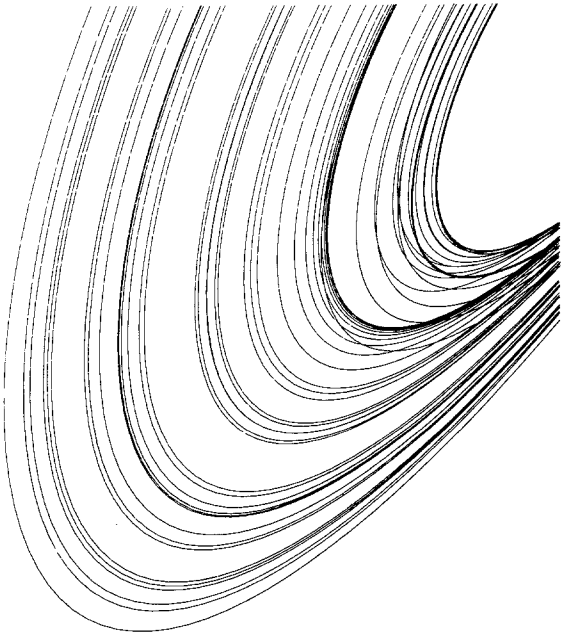

Fig. 10 (*continued*)

Two other stable orbits, B and C, were discovered for this system, born in saddle-node bifurcations at $r \approx 64.31$ and $r \approx 75.7$, respectively, and both symmetric. Refer to Fig. 8 for illustrations of A, B, and C, and Fig. 9 for a bifurcation diagram. The stable ranges of B and C are terminated by symmetry-breaking bifurcations with associated series of period doublings. Some of the doubled orbits and chaotic solutions associated with orbit B are depicted in Fig. 10. Note that all the bifurcations here are supercritical, lending the bifurcation diagram a much more uniform appearance than the one in Section 5.1. A comprehensive list of r values at which bifurcations take place is presented in Table III.

Such sequences of period-doubled solutions were first observed in one-dimensional maps, for which Feigenbaum[20] showed that if the nth period doubling occurs at parameter value $r = r_n$, then

$$\frac{r_n - r_{n-1}}{r_{n+1} - r_n} \to \delta \qquad \text{as} \quad n \to \infty \tag{5.1}$$

where $\delta \approx 4.6692...$ is a universal constant. Computation of the left-hand side of (5.1) for the values listed in Table III, and also the doubled orbits generated by orbits D, E, F of the previous section, shows that (5.1) appears also to hold for the system of ordinary differential equations (2.14). Although (5.1) has not been proved to apply to systems of ordinary differential equations, its apparent validity has been observed in other truncated systems.[5,21]

6. CONCLUSIONS

A general pattern can be perceived in the results of the previous section. The first oscillatory branch of solutions appears in a Hopf bifurcation from either the conduction solution or the stationary convective solution. After it has given way to chaos, further oscillatory solutions are generated at saddle-node bifurcations and disappear at symmetry-breaking bifurcations (if symmetric) or period-doubling bifurcations (if asymmetric). The general impression is of a series of stable orbits punctuated by short chaotic regions. Contrast the Lorenz equations, where narrow periodic windows separate chaotic solutions stable over large r intervals. We conclude that the effect of adding rotation to the Lorenz model is not only to delay the onset of convection as predicted by linear theory, but also to enhance stability above convective onset by favoring oscillatory solutions. Of course, in a real fluid, relaminarization at high Rayleigh number would not be observed.

The rotating system (2.14) provides examples of subcritical symmetry-

breaking bifurcations and sizable regions where two different oscillatory solutions are simultaneously stable, allowing the possibility of hysteretic transitions between them.

The large-r analysis demonstrates that special behavior occurs when $d^2 < (b+2)/b$ and σ is just less than $(b+1)/(d^2+1)$. Thus, equations (2.14) provide an explicit example of a system where certain phenomena are restricted to a small region in parameter space. Evidence that this large-r behavior influences behavior at much lower values of r, at least when $\sigma > \sigma_0$, is provided by the apparent link with the occurrence of two Hopf bifurcations on the steady branch. The conditions for anomalous large-r behavior can also be satisfied when $\sigma < \sigma_0$, particularly if b is small.

Finally, we reiterate that the four-mode model is expected to give good qualitative agreement with the results of future experiments on rotating convective layers and predicts phenomena not previously observed experimentally in other systems.

APPENDIX A.

Analysis of small-amplitude oscillations bifurcating from the conduction solution at $r = r^{(0)}$ proceeds as follows. For periodic motion with frequency ω, differentiation with respect to time is equivalent to multiplication by $i\omega$. Expanding in terms of a parameter ε which measures the amplitude of convection, we have

$$\begin{aligned} \omega &= \omega_0 + \varepsilon\omega_1 + \varepsilon^2\omega_2 + \cdots \\ r &= r_0 + \varepsilon r_1 + \varepsilon^2 r_2 + \cdots \\ x &= \varepsilon x_1 + \varepsilon^2 x_2 + \varepsilon^3 x_3 + \cdots \\ y &= \varepsilon y_1 + \varepsilon^2 y_2 + \varepsilon^3 y_3 + \cdots \\ z &= \varepsilon z_1 + \varepsilon^2 z_2 + \varepsilon^2 z_3 + \cdots \\ w &= \varepsilon w_1 + \varepsilon^2 w_2 + \varepsilon^3 w_3 + \cdots \end{aligned} \tag{A1}$$

Substitution of the expansion (A1) into the governing equations (2.14) gives at first order

$$\mathsf{L}_0 \begin{pmatrix} x_1 \\ y_1 \\ w_1 \end{pmatrix} \equiv \begin{pmatrix} i\omega_0 + \sigma & -\sigma & -\sigma d \\ -r_0 & i\omega_0 + 1 & 0 \\ \sigma d & 0 & i\omega_0 + \sigma \end{pmatrix} \begin{pmatrix} x_1 \\ y_1 \\ w_1 \end{pmatrix} = 0 \tag{A2}$$

together with $z_1 = 0$. A nontrivial solution requires $\det(\mathsf{L}_0) = 0$.

Equating real and imaginary parts reproduces (3.3) and (3.4). An

alternative way of expressing this condition[8] (which will prove useful in later stages of the calculation) is

$$\mathbf{M}_0 \cdot \mathsf{L}_0 = 0 \tag{A3}$$

where $\mathbf{M}_0$ is the first row of a matrix which reduces L_0 to lower triangular form. In this instance

$$\mathbf{M}_0 = ((i\omega_0 + 1)(i\omega_0 + \sigma),\ \sigma(i\omega_0 + \sigma),\ \sigma d(i\omega_0 + 1)) \tag{A4}$$

Equation (A2) can be solved for (x_1, y_1, w_1) up to a normalization factor

$$x_1 = e^{i\omega t}, \qquad y_1 = \frac{r_0 e^{i\omega t}}{i\omega_0 + 1}, \qquad w_1 = -\frac{\sigma d e^{i\omega t}}{i\omega_0 + \sigma} \tag{A5}$$

At second order we find

$$\mathsf{L}_0 \begin{pmatrix} x_2 \\ y_2 \\ w_2 \end{pmatrix} = \begin{pmatrix} -i\omega_1 x_1 \\ -i\omega_1 y_1 + r_1 x_1 \\ -i\omega_1 w_1 \end{pmatrix} \tag{A6}$$

Multiplying by $\mathbf{M}_0$ and taking real and imaginary parts gives $r_1 = \omega_1 = 0$. Any nonzero solution of (A6) for (x_2, y_2, w_2) is now seen to be a multiple of (x_1, y_1, w_1) and could therefore be incorporated in the first-order term. Thus we may take $x_2 = y_2 = w_2 = 0$. The associated equation for z_2 is

$$\dot{z}_2 + bz_2 = x_1 y_1 \tag{A7}$$

Representation of physical quantities by the real part of a complex expression may be maintained, despite the introduction of nonlinear terms, using a trick due to Knobloch *et al.*[8]: the product of two variables $z_1 z_2$ is written as $z_1(z_2 + z_2^*)/2$. We find

$$z_2 = \frac{r_0}{2b(i\omega_0 + 1)}\left(1 + \frac{be^{2i\omega t}}{2i\omega + b}\right) \tag{A8}$$

At third order

$$\mathsf{L}_0 \begin{pmatrix} x_3 \\ y_3 \\ w_3 \end{pmatrix} = \begin{pmatrix} -i\omega_2 x_1 \\ -i\omega_2 y_1 + r_2 x_1 - x_1 z_2 \\ -i\omega_2 w_1 \end{pmatrix} \tag{A9}$$

It is convenient to use the above technique to evaluate $x_1 z_2$ in such a way that $e^{-i\omega t}$ terms are eliminated in favor of $e^{i\omega t}$ terms. The need to avoid

breakdown of the whole perturbation scheme due to the appearance of nonperiodic terms in the solution for (x_3, y_3, w_3) is expressed by the solvability condition or Fredholm alternative,[14]

$$\mathbf{M}_0[\text{terms in rhs of (A9)} \propto e^{i\omega t}] = 0 \tag{A10}$$

Elimination of r_0 and d^2 in favor of ω_0 using

$$r_0 = \frac{2(1+\omega_0^2)}{1-\sigma}, \qquad d^2 = \frac{(\omega_0^2+\sigma^2)(1+\sigma)}{\sigma^2(1-\sigma)} \tag{A11}$$

simplifies (A10) to yield

$$\begin{aligned} &2\omega_0\omega_2(1+2\sigma+i\omega_0) + \sigma r_2(i\omega_0+\sigma) \\ &\quad = \frac{\sigma}{1-\sigma}(i\omega_0+\sigma)\left(\frac{1}{b}+\frac{1}{2}\frac{1-i\omega_0}{2i\omega_0+b}\right) \end{aligned} \tag{A12}$$

Given a particular set of parameter values, the real and imaginary parts of (A12) may be solved for r_2 and ω_2. Of particular interest, however, is the transition between supercriticality and subcriticality which occurs when ω_2 is real at $r_2 = 0$. This condition reduces to

$$\omega_0^2 = \frac{\sigma(1+2\sigma)\,b(b+2) - 3b^2(1+\sigma)}{2(4-b)(1+\sigma) - b(b+2)} \tag{A13}$$

A similar calculation for the Hopf bifurcation from steady convection gives the solvability criterion

$$\begin{aligned} &-i\omega_2(M_{01}x_1 + M_{02}x_2 + M_{03}x_3 + M_{04}x_4) \\ &\quad + s_2\{-M_{02}z_1 + M_{03}[(1+d^2)\,x_1 + y_1]\} \\ &\quad + [-M_{02}(x_1z_2 + x_2z_1) + M_{03}(x_1\,y_2 + y_1x_2)] = 0 \end{aligned} \tag{A14}$$

where

$$\begin{aligned} M_{01} &= (i\omega_0+1)(i\omega_0+b)(i\omega_0+\sigma) + s_0^2(i\omega_0+\sigma) \\ M_{02} &= (i\omega_0+b)(i\omega_0+\sigma)\,\sigma \\ M_{03} &= -s_0\sigma(i\omega_0+\sigma) \\ M_{04} &= \sigma d[(i\omega_0+1)(i\omega_0+b) + s_0^2] \end{aligned} \tag{A15}$$

and

$$x_1 = e^{i\omega t}$$

$$y_1 = \frac{1}{\sigma}\left[(i\omega_0 + \sigma) + \frac{\sigma^2 d^2}{i\omega_0 + \sigma}\right] e^{i\omega t}$$

$$z_1 = \left\{\frac{1+d^2}{s_0} - \frac{i\omega_0 + 1}{\sigma s_0}\left[(i\omega_0 + \sigma) + \frac{\sigma^2 d^2}{i\omega_0 + \sigma}\right]\right\} e^{i\omega t} \tag{A16}$$

$$w_1 = -\frac{\sigma d}{i\omega_0 + \sigma} e^{i\omega t}$$

and the nonlinear terms are

$$x_1 z_2 = \left(\frac{1}{2}E + F\right) e^{i\omega t} \tag{A17}$$

$$z_1 x_2 = \frac{1}{2}\left\{\frac{1+d^2}{s_0} - \frac{1 - i\omega_0}{\sigma s_0}\left[(\sigma - i\omega_0) + \frac{\sigma^2 d^2}{\sigma - i\omega_0}\right]\right\} A e^{i\omega t}$$

$$+ \left\{\frac{1+d^2}{s_0} - \frac{1 + i\omega_0}{\sigma s_0}\left[(\sigma + i\omega_0) + \frac{\sigma^2 d^2}{\sigma + i\omega_0}\right]\right\} B e^{i\omega t} \tag{A18}$$

$$x_1 y_2 = \left(\frac{1}{2}C + D\right) e^{i\omega t} \tag{A19}$$

$$y_1 x_2 = \frac{1}{2\sigma}\left((\sigma - i\omega_0) + \frac{\sigma^2 d^2}{\sigma - i\omega_0}\right) A e^{i\omega t}$$

$$+ \frac{1}{\sigma}\left((\sigma + i\omega_0) + \frac{\sigma^2 d^2}{\sigma + i\omega_0}\right) B e^{i\omega t} \tag{A20}$$

where only terms proportional to $\exp(i\omega t)$ have been retained. Defining $K = 1 + d^2$, we can determine the coefficients A to F from the equations

$$-KA + (2i\omega + 1)\, C + s_0 E$$

$$= \frac{1}{2s_0}\left\{-K + \frac{i\omega_0 + 1}{\sigma}\left[(i\omega_0 + \sigma) + \frac{\sigma^2 d^2}{i\omega_0 + \sigma}\right]\right\} \tag{A21}$$

$$-Ks_0 A - s_0 C + (2i\omega + b)\, E$$

$$= \frac{1}{2\sigma}\left[(i\omega_0 + \sigma) + \frac{\sigma^2 d^2}{i\omega_0 + \sigma}\right] \tag{A22}$$

$$B = \frac{1}{2Ks_0}\left[bF - \frac{1}{2}\left(1 + \frac{\sigma^2 d^2}{\sigma^2 + \omega_0^2}\right)\right] \tag{A23}$$

$$C = \frac{1}{\sigma}\left[(2i\omega_0 + \sigma) + \frac{\sigma^2 d^2}{2i\omega_0 + \sigma}\right] A \tag{A24}$$

$$D = KB \tag{A25}$$

$$F = -\frac{1}{2s_0^2}\left(K + \frac{\omega_0^2 - \sigma}{\sigma} - \sigma d^2 \frac{\sigma + \omega_0^2}{\sigma^2 + \omega_0^2}\right) \tag{A26}$$

Solving the two equations which comprise the real and imaginary parts of (A13) determines ω_2 and s_2, a tedious piece of algebra delegated to a computer.

When $\sigma = 10$, $b = 8/3$, and $d = 0$, our computer program gives $r - r_H = -0.02144\varepsilon^2$, in excellent agreement with Rowlands' multitime analysis of the basic Lorenz equations.[15]

APPENDIX B

This Appendix gives details of the calculations outlined in Section 4. We wish first of all to integrate equations (4.8). From (4.8c) and (4.9)

$$Z' = [2(B - Z)(Z + B)(Z + A)]^{1/2} \tag{B1}$$

which has solution (see Byrd and Friedman,[17] §236)

$$Z = B(1 - 2\,\mathrm{sn}^2 u), \qquad \text{where} \quad u = [(A + B)/2]^{1/2}\,\tau \tag{B2}$$

and the modulus k is given by

$$k^2 = \frac{2B}{A + B} \tag{B3}$$

This solution is valid provided $0 < k < 1$, i.e., $A > B > 0$. In the region $|A| < B$, reordering the factors in (B1) allows the solution

$$\begin{aligned} Z &= B - (A + B)\,\mathrm{sn}^2 u, \qquad u = B^{1/2}\tau \\ k^2 &= \frac{A + B}{2B} \end{aligned} \tag{B4}$$

ξ and η are determined from (4.9) and (4.8a):

$$\left.\begin{aligned} \xi &= \pm 2^{1/2}(A + B)^{1/2}\,\mathrm{dn}\,u \\ \eta &= \mp 2B\,\mathrm{sn}\,u\,\mathrm{cn}\,u \end{aligned}\right\}, \qquad A > B > 0 \tag{B5}$$

$$\left.\begin{aligned} \xi &= \pm 2^{1/2}(A + B)^{1/2}\,\mathrm{cn}\,u \\ \eta &= \mp 2kB\,\mathrm{sn}\,u\,\mathrm{dn}\,u \end{aligned}\right\}, \qquad |A| < B \tag{B6}$$

Due to the periodicity of the elliptic functions, these solutions are periodic orbits, periods $2K$ and $4K$, respectively. If $|A| < B$, increasing u by $2K$ maps (ξ, η, Z, μ) to $(-\xi, -\eta, Z, -\mu)$ and the orbit is symmetric. (Although $\mu = C$, we show below that $C = 0$ if $|A| < B$). Naturally, the symmetry properties of orbits are unaffected by the rescaling (4.6). Conversely if $A > B > 0$, increasing u by K reveals the solution to be asymmetric. Either way, we may make a choice of sign; in (B6) the upper and lower signs represent the same orbit, while in (B5) the two signs represent orbits which are mapped into each other by the symmetry.

Proceeding to the situation where ε is small but finite, the average rate of change of A in the time interval $\Delta\tau$ is

$$\frac{\Delta A}{\Delta\tau} = \frac{1}{\Delta\tau} \int_{u(\tau)}^{u(\tau+\Delta\tau)} \frac{dA}{d\tau} \frac{d\tau}{du}\, du \tag{B7}$$

$dA/d\tau$ is given by (4.10) and is $O(\varepsilon)$. Writing $u = \alpha\tau$, where $\alpha = [1/2(A+B)]^{1/2}$ or $B^{1/2}$, we may set $\Delta u = \alpha\Delta\tau$ and $d\tau/du = 1/\alpha$ in (B7), incurring an error of order ε^2, which is negligible. Thus,

$$\frac{\Delta A}{\Delta\tau} = \frac{1}{\Delta u} \int_{u(\tau)}^{u(\tau+\Delta\tau)} \frac{dA}{d\tau}\, du \tag{B8}$$

Similar equations apply for B and C. Substituting from (4.10) and integrating gives the averaged equations

$$\begin{aligned}
KA' &= \varepsilon \left\{ b\sigma K - \frac{4B\sigma}{k^2} E - \frac{bB}{k^2} [(2-k^2) K - 2E] + \frac{\pi B^{1/2}}{k} \sigma d C \right\} \\
3Kk^4 B' &= -\varepsilon \{ 4B[(2-k^2) E - 2(1-k^2) K] \\
&\quad + bB[4(k^2-2) E + (3k^4 - 8k^2 + 8) K] \\
&\quad + 3b\sigma k^2 [2E - K(2-k^2)] \} \\
KC' &= -\varepsilon \left(\sigma C K + \frac{B^{1/2}}{k} \sigma d\pi \right) \qquad (A > B > 0)
\end{aligned} \tag{B9}$$

and

$$\begin{aligned}
KA' &= \varepsilon \{ Kb\sigma + bB(2E - K) - 4B\sigma[E - (1-k^2) K] \} \\
3KB' &= -\varepsilon \{ 4B[K(1-k^2) + E(2k^2 - 1)] + 3b\sigma(2E - K) \\
&\quad + bB[K(4k^2 - 1) + 4E(1 - 2k^2)] \} \\
C' &= -\varepsilon\sigma C \qquad (|A| < B)
\end{aligned} \tag{B10}$$

The constants K and E are complete elliptic integrals of the first and second kind.

In the regime $|A| < B$, stationary points occur only if $C = 0$, and solutions with $C \neq 0$ tend exponentially to the $C = 0$ plane. The first two equations in (B10) are then identical to those derived for the Lorenz model by Sparrow,[16] so the behavior in $|A| < B$ is unaffected by rotation. Sparrow introduced the parameter $\lambda = (\sigma + 1)/(b + 2)$ and showed that a unique stationary point existed if and only if $\lambda > 2/3$.

In the other regime, $A > B > 0$, setting $C' = 0$ gives

$$C = -\frac{B^{1/2}\, d\pi}{kK} \tag{B11}$$

Substituting in the equation $A' = 0$, we have

$$0 = b\sigma K - \frac{4B\sigma}{k^2} E - \frac{bB}{k^2}\left[(2 - k^2)\, K - 2E\right] - \sigma \frac{d^2\pi^2 B}{k^2 K} \tag{B12}$$

As it can be shown that the term in square brackets is positive, Eq. (B12) determines a unique value for B. Inserting this value into the equation $B' = 0$ produces a condition relating k to σ, b, and d. It does not appear possible to write this condition concisely in terms of a parameter such as λ. Instead, solving for σ, we obtain

$$\sigma = \frac{b + (b + 2)\, f(E, K, k)}{2 + \pi^2 d^2 / 2KE} \tag{B13}$$

where

$$f(E, K, k) = \frac{K\left[(2 - k^2)\, E - 2(1 - k^2)\, K\right]}{3E\left[(2 - k^2)\, K - 2E\right]} \tag{B14}$$

When $k = 0$, the right-hand side of (B13) equals $(b + 1)/(d^2 + 1)$. As $k \to 1$, $K \to \infty$ logarithmically and $E(1) = 1$, so the right-hand side tends to infinity. We conclude that there exists at least one stationary point for $\sigma > (b + 1)/(d^2 + 1)$. If k is small, (B13) and (B14) can be expanded as power series in k^2, using the series expansions for E and K in Byrd and Friedman,[17] §900. Retaining terms of order k^4, we have

$$(1 + d^2)\, \sigma = b + 1 + \frac{1}{64} k^4 \frac{bd^2 - b - 2}{1 + d^2} \tag{B15}$$

If $d^2 < (b + 2)/b$, the expression for σ is a decreasing function of k for k just above 0. It must subsequently pass through a minimum before increasing

again in order to become infinite at $k = 1$. Numerical calculation of this expression using NAG routines S21BBF and S21BCF shows it to have no other turning points. Because the k^2 term in (B15) is identically zero, the minimum is rather shallow and no stationary points exist when σ is appreciably less than $(b+1)/(d^2+1)$.

The boundaries of the two regimes are defined by the relations $B = 0$, $A = -B$, and $A = B$. When $A = \pm B$, the averaged equations assume the same form as in the nonrotating problem, and need not concern us further. On the line $B = 0$, $k = 0$ and $K = E = \pi/2$. The averaged equations reduce to

$$\begin{aligned} A' &\sim \varepsilon\sigma[b - 2A(1+d^2)] \\ B' &\sim \tfrac{1}{4}\varepsilon B(b\sigma/A - 2b - 2) \end{aligned} \tag{B16}$$

with a stationary point at $A = b/2(1+d^2)$, $B = 0$. The stationary point is stable provided $\sigma < (b+1)/(d^2+1)$, whereupon trajectories with small, positive B decay toward $B = 0$.

ACKNOWLEDGMENTS

I thank A. J. McKane for valuable advice and G. S. Mani for writing the orbit-plotting program. Receipt of an SERC studentship is acknowledged.

REFERENCES

1. E. Knobloch, D. R. Moore, J. Toomre, and N. O. Weiss, *J. Fluid Mech.* **166**:409–448 (1986).
2. E. N. Lorenz, *J. Atmos. Sci.* **20**:130–141 (1963).
3. G. Veronis, *J. Fluid Mech.* **24**:545–554 (1966).
4. V. Franceschini and C. Boldrighini, *Commun. Math. Phys.* **64**:159–170 (1979).
5. V. Franceschini and C. Tebaldi, *J. Stat. Phys.* **21**:707–726 (1979).
6. J. H. Curry, *Commun. Math. Phys.* **60**:193–204 (1978).
7. L. N. Da Costa, E. Knobloch, and N. O. Weiss, *J. Fluid Mech.* **109**:25–43 (1981).
8. E. Knobloch, N. O. Weiss, and L. N. Da Costa, *J. Fluid Mech.* **113**:153–186 (1981).
9. P. H. Coullet and E. A. Spiegel, *SIAM J. Appl. Math.* **43**:776–821 (1983).
10. A. Arneodo, P. H. Coullet, and E. A. Spiegel, *Geophys. Astrophys. Fluid Dynam.* **31**:1–48 (1985).
11. R. M. Clever and F. H. Busse, *J. Fluid Mech.* **94**:609–627 (1979).
12. G. Z. Gershuni and E. M. Zhukhovitskii, *Convective Stability of Incompressible Fluids* (Israel Program for Scientific Translations, Jerusalem, 1976).
13. J. K. Bhattacharjee and A. J. McKane, *J. Phys. A* **21**:L555–L558 (1988).
14. G. Iooss and D. D. Joseph, *Elementary Stability and Bifurcation Theory* (Springer, New York, 1980).

15. G. Rowlands, *J. Phys. A* **16**:585–590 (1983).
16. C. T. Sparrow, *The Lorenz Equations: Bifurcations, Chaos and Strange Attractors* (Springer, New York, 1982).
17. P. F. Byrd and M. D. Friedman, *Handbook of Elliptic Integrals for Engineers and Scientists* (Springer, New York, 1971).
18. J. H. Curry, in *Global Theory of Dynamical Systems*, Z. Nitecki and C. Robinson, eds. (Springer, New York, 1979).
19. P. Glendinning and C. T. Sparrow, *J. Stat. Phys.* **35**:645–696 (1984).
20. M. J. Feigenbaum, *J. Stat. Phys.* **19**:25–52 (1978).
21. V. Franceschini, *J. Stat. Phys.* **22**:397–406 (1980).